IN SITU SYNCHROTRON X-RAY TECHNIQUES FOR THE STUDY OF LITHIUM BATTERY MATERIALS

J. McBreen, S. Mukerjee X. Q. Yang, and X. Sun
Department of Applied Science
Brookhaven National Laboratory
Upton, NY 11973

Y. Ein-Eli
Covalent Associates, Inc.
Woburn, MA 01801

ABSTRACT

The combination of in situ X-ray diffraction (XRD) and x-ray absorption spectroscopy (XAS) is a very powerful technique in the study of lithium battery cathode materials. XRD identifies the phase changes that occur during cycling and XAS gives information on the redox charge compensation processes that occur on the transition metal oxides. Because of its element specific nature XAS can identify the occurrence of redox processes on the various cations in doped oxide cathode materials. Since XAS probes short range order and is particularly useful in the study of amorphous tin based composite oxide anode materials.

INTRODUCTION

Electrochemists, and in particular battery researchers, have long recognized the need to obtain structural information *in situ*. One of the earliest reports of an *in situ* x-ray experiment was in the late fifties when Andrews and Ubbelhode (1) did an *in situ* x-ray diffraction (XRD) study of the formation of palladium hydride in an electrochemical cell. Shortly after that Salkind and Bruins (2), Falk (3) and Briggs (4,5) did *in situ* XRD on nickel hydroxide electrodes. The technique was not widely applied because of the limitations of conventional x-ray sources and the difficulty of the experiments. With the advent of computer controlled experiments and data acquisition there was renewed interest in the technique and several publications appeared in the late seventies and early eighties (6-11). Further advances have been made through the use of cleverly designed cells that reduce the attenuation of the x-rays, and in recent years there have been reports of *in situ* XRD studies of $LiMn_2O_4$ (12), $LiNiO_2$ (13) and $LiCoO_2$ (14). The advent of synchrotron x-ray sources with high brightness also makes it possible to do surface x-ray diffraction using grazing incidence x-ray geometry (15).

Work on x-ray absorption spectroscopy (XAS) started about the same time x-ray diffraction, and was used extensively in the early decades of this century to elucidate the structure of the inner electron shells of the elements. The most notable work was that of Moseley, who determined the atomic numbers of the elements from x-ray fluorescence (16). The extended x-ray absorption fine structure (EXAFS) was first observed in 1920 (17). However, there was very little progress on the field until the seventies. The main inhibition to development of the field was the lack of a sufficiently intense tunable x-ray source. Then

the only available source was the bremsstrahlung from conventional x-ray tubes. The intensity of the bremsstrahlung is typically a hundred times lower than the intensity of the K_α peaks that are used for XRD. In an XAS experiment the signal to noise ratio is proportional to the square root of the x-ray spectral brightness. The lack of x-ray sources of sufficient spectral brightness prevented the verification of several proposed theories for the EXAFS. A major breakthrough in the origin of the EXAFS came in 1971 when Sayers *et al.* showed that the Fourier transform of the EXAFS data with respect to the photoelectron vector yields a radial structure function in which the locations of the various peaks are related to nearest neighbor distances of the local structural environment in the crystal (18). The availability of intense synchrotron x-ray sources in the late seventies and early eighties greatly increased activity in the area. These sources yielded x-ray intensities that were as much as seven orders of magnitude greater that that from the brehmstralung of conventional x-ray tubes. Now it became possible to use the EXAFS technique as a powerful tool in the determination of short-range structural parameters such as coordination distances and coordination numbers. The x-ray absorption near edge structure (XANES) also provides useful chemical information such as oxidation states and coordination symmetry.

The combination of *in situ* XAS and XRD is particularly powerful in the study of lithium battery materials. The *in situ* measurements can easily be done since both the probe and signal are penetrating x-rays. A major advantage of XAS is that it is element specific. In cathode materials such as $LiNi_{1-x}Co_xO_2$ it is possible to do measurements at both the Ni and Co K edges and determine the redox behavior of the Ni and Co at various stages of charge and discharge. Since XAS probes only short-range order it can be used to study amorphous tin-based composite oxide (TCO) anode materials such as $SnB_{0.56}P_{0.4}Al_{0.42}O_{3.47}$. *In situ* XRD can elucidate the phase changes that occur during electrode cycling. This paper will illustrate examples of the application of the combination of in situ XAS and XRD to study cathode materials.

EXPERIMENTAL

Spectroelectrochemical cell

The techniques used for *in situ* XAS on electrodes for aqueous batteries have been described in detail previously (4-6). With non-aqueous systems the techniques are similar except that provisions have to be made to hermetically seal the cell. For transmission XAS measurements it is necessary to have uniform x-ray absorption throughout the electrode. For this reason electrodes with metallic grid current collectors are not suitable. The cathodes were made by made by casting a mixture of the cathode material ($LiCu_{0.5}Mn_{1.5}O_4$ or $LiNi_{0.5}Mn_{1.5}O_4$), an acetylene black conductive diluent and a binder (PVdF in a fugitive solvent) on to an aluminum foil sheet. Disc electrodes (2.82 cm^2) were punched from the sheet and were incorporated in the cell with a Celgard separator and a lithium foil anode. The electrolyte was 1 M $LiPF_6$ in solvent mixture of 1EC:3EMC.

In situ XRD and XAS measurements

In situ XRD measurements were conducted in the transmission mode at Beam Line X18A of NSLS, using a 10.375 KeV ($\lambda = 1.195$ Å) x-ray beam. Successive scans were

DISCLAIMER

DISCLAIMER

Portions of this document may be illegible
in electronic image products. Images are
produced from the best available original
document.

taken between 2θ values of 43° to 53° as the cells were cycled at 50 μA/cm². The scans included the (331) and the (511) peaks of the spinel, which coincide, as well as the (440) and (531) peaks. Also included was the aluminum (220) peak, which served as an internal calibration.

In a separate experiment in situ XAS measurements, at the Mn, Ni and Cu K edges, were done at Beam Line X11A at NSLS. These experiments were also done in the transmission mode with three ionization chamber detectors. Either a Mn, Ni or Cu reference foil was used in conjunction with the third detector for calibration of edge positions. The beam was detuned by 50% at the Mn K edge and 15% at the Ni and Cu K edges to reject higher harmonics.

RESULTS AND DISCUSSION

$LiCu_{0.5}Mn_{1.5}O_4$

Figure 1 shows a typical charge/discharge curve for $LiCu_{0.5}Mn_{1.5}O_4$. On charge there was a sloping voltage plateau between 3.8 and 4.4 V followed by a higher voltage at 4.95 V. In spite of the high voltage there was good coulombic efficiency and very little electrolyte decomposition. The capacity maintenance was excellent over 220 deep cycles.

Figures 2 and 3 show the XRD patterns obtained during charge and discharge. During charge, on the lower plateau the diffraction peaks shift to higher angles, indicating a contraction of the lattice on the removal of lithium ions. On the higher plateau there was no further contraction of the lattice. The whole process occurs in a single phase. No line broadening or peak splitting that would be indicative of the formation of a second phase was observed. In the case of $LiMn_2O_4$ three, phases are observed. The data in Fig. 3 indicate that the process is highly reversible. The highly reversible single-phase behavior accounts for the excellent stability of the electrode during cycling.

Figure 4 shows the Mn K edge XANES during charge. The shifts in the edge position in the 3.8 to 4.5 volt region are consistent with the oxidation of residual Mn(III) to Mn(IV). On the upper plateau there is no further edge shift, indication that Mn does not participate in the charge compensation mechanism in this region. There are changes in the white line in the 4.8 to 5 V region. These are consistent with changes in coordination symmetry with the egress of more lithium ions. Figure 5 shows the Cu K edge XANES during charge. On the lower voltage plateau there is very little change in the Cu XANES, indicating that Cu does not participate in the reaction. On the upper plateau very large changes, consistent with the oxidation of Cu(II) to Cu(III) are observed. This indicates that on the upper plateau the charge compensation mechanism occurs on Cu.

$LiNi_{0.5}Mn_{1.5}O_4$

Work by Amine et al. showed that substitution of Mn by Ni, to the extent of $LiNi_{0.5}Mn_{1.5}O_4$, stabilized electrode operation on the 3 V plateau and prevented the formation of the tetragonal phase on the lower plateau (19). Later Dahn and co-workers discovered that substitution of Mn with Ni decreased the length of the 4 V plateau and

resulted in a new plateau at 4.7 V (20). Ni substitution, to the extent of $LiNi_{0.5}Mn_{1.5}O_4$, completely eliminated the 4 V plateau.

Figure 6 shows a typical charging curve for $LiNi_{0.5}Mn_{1.5}O_4$ charged at the C/10 rate. Figure 7 shows a set of XRD scans obtained during the second charge. The data indicates the presence of three cubic phases. The lattice parameters are given in Fig. 8. The data indicate the occurrence of two first order phase transitions.

Figure 9 shows the Mn K edge XANES as a function of charging time. Unlike $LiCu_{0.5}Mn_{1.5}O_4$ there is little if any residual Mn(III). The Mn starts off as Mn(IV) and no further oxidation occurs. Figure 10 shows the Ni K edge XANES as a function of charging time. The data clearly indicate that, on the plateau at 4.8 V, essentially all of the charge compensation occurs on the Ni atoms.

CONCLUSION

In recent lithium battery cathode development there has been a trend toward the use of oxide cathodes with two or more transition metal cations. The present work shows that XAS is an excellent technique for determining the behavior of the various cations during the intercalation/deintercalation process. It is possible to determine order in which cations are oxidized and the variations in the electronic and coordination structure around cations in the oxide during the electrochemical deintercalation of lithium.

ACKNOWLEDGMENT

REFERENCES

1.   J. N. Andrews and A. R. Ubbelhode, *Proc. Roy. Soc.*, **A253**, 6 (1959).

1.   A. J. Salkind and P. F. Bruins, *J. Electrochem. Soc.*, **109**, 256 (1962).

3.   S. U. Falk, *J. Electrochem. Soc.*, **107**, 661 (1960).

4.   G. W. D. Briggs, *Electrochim. Acta*, **1**, 297 (1959).

5.   G. W. D. Briggs and W. F. K. Wynne-Jones, *Electrochim. Acta*, **7**, 241 (1962).

6.   R. R. Chianelli, J. C. Scanlon and B. M. L. Rao, **125**, 1563 (1978).

7.   M. Fleischman, A. Oliver and J. Robinson, *Electrochim. Acta*, **31**, 899 (1986).

8.   M. Fleischman and B. W. Mao, *J. Electroanal. Chem.* **229**, 125 (1987).

9.   K. Machida and M. Enyo, *Bull. Chem. Soc. Jpn.*, **62**, 415 (1989).

10.   G. Nazri and R. H. Muller, *J. Electrochem. Soc.*, **132**, 1385. (1985).

11.   N. G. Sudorgin and V. B. Nalbandyan, *Élektrokhimiya*, **28**, 122 (1992).

12.   M. N. Richard, I. Koetschau and J. R. Dahn, *J. Electrochem. Soc.*, **144**, 554 (1997).

13.   W. Li, J. N. Reimers and J. R. Dahn, *Solid State Ionics,* **67**, 123 (1993).

14.   G. Amatucci, J. M. Tarascon and L. C. Klein, *J. Electrochem. Soc.*, **143**, 1114 (1996).

15.   M. F. Toney, and O. R. Melroy, in *Electrochemical Interfaces: Modern Techniques for In-Situ Interface Characterization,* H. D. Abruña, Editor, p. 55, VCH Publishers, Inc., New York (1991).

16.   H. G. J. Moseley, *Phil. Mag,* **26**, 1024 (1913); **27**, 703 (1914).

17.   H. Fricke, *Phys. Rev.*, **16**, 202 (1920).

18.   D. E. Sayers, E. A. Stern and F. W. Lytle, *Phys. Rev. Lett.*, **27**, 1204 (1971).

19.   K. Amine, H. Tukamoto, H. Yasuda and Y. Fujita, *J. Electrochem. Soc.*, **143**, 1607 (1996).

20   Q. Zhong, A. Bonakdarpour, M. Zhang, Y. Gao and J. R. Dahn, *J. Electrochem. Soc.*, **144**, 205 (1997).
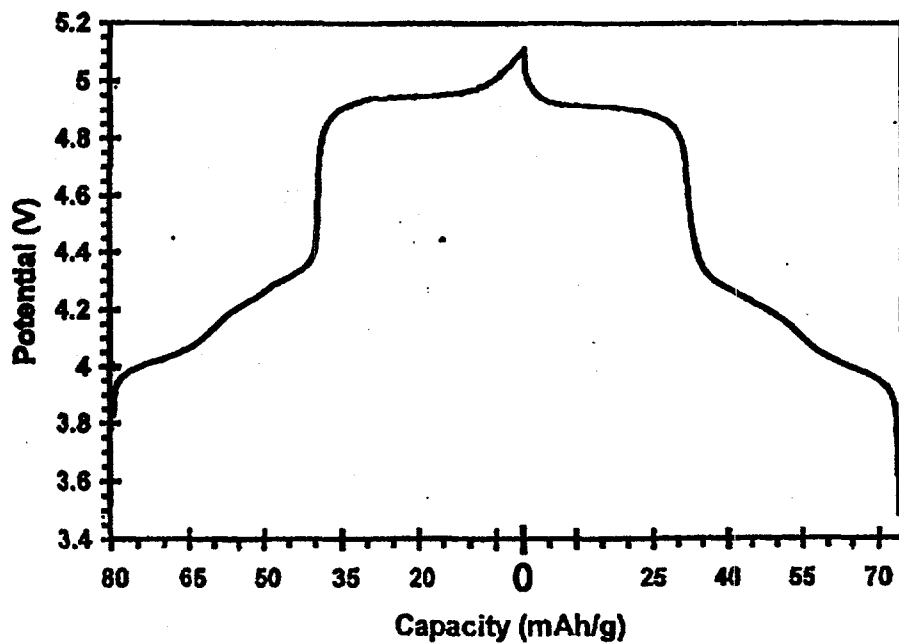
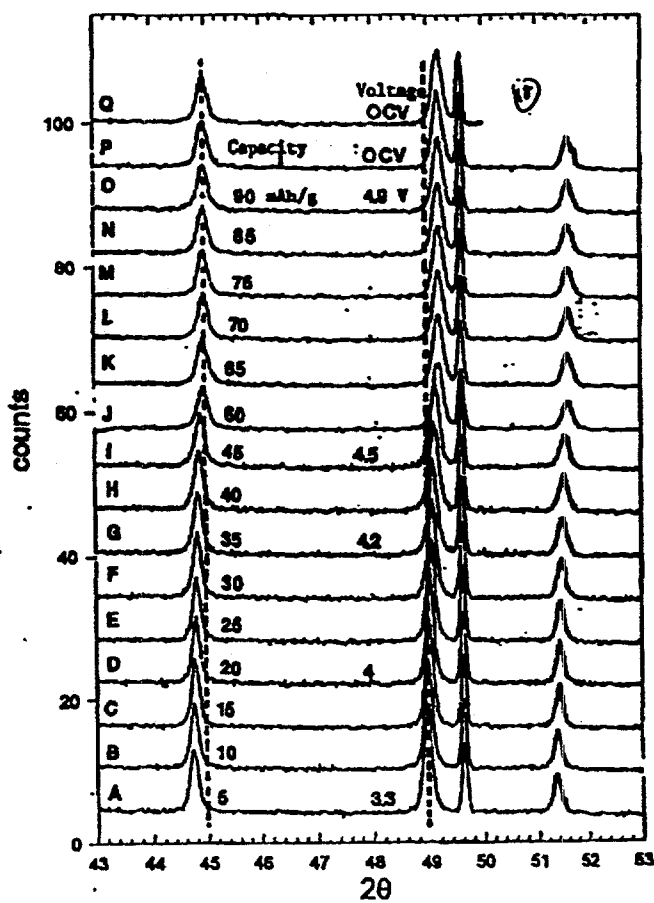Fig. 1 Charge/discharge curve for Li/LiCu$_{0.5}$Mn$_{1.5}$O$_4$ cell.

Fig. 2. *In situ* XRD patterns on LiCu$_{0.5}$Mn$_{1.5}$O$_4$ during the second charge cycle.

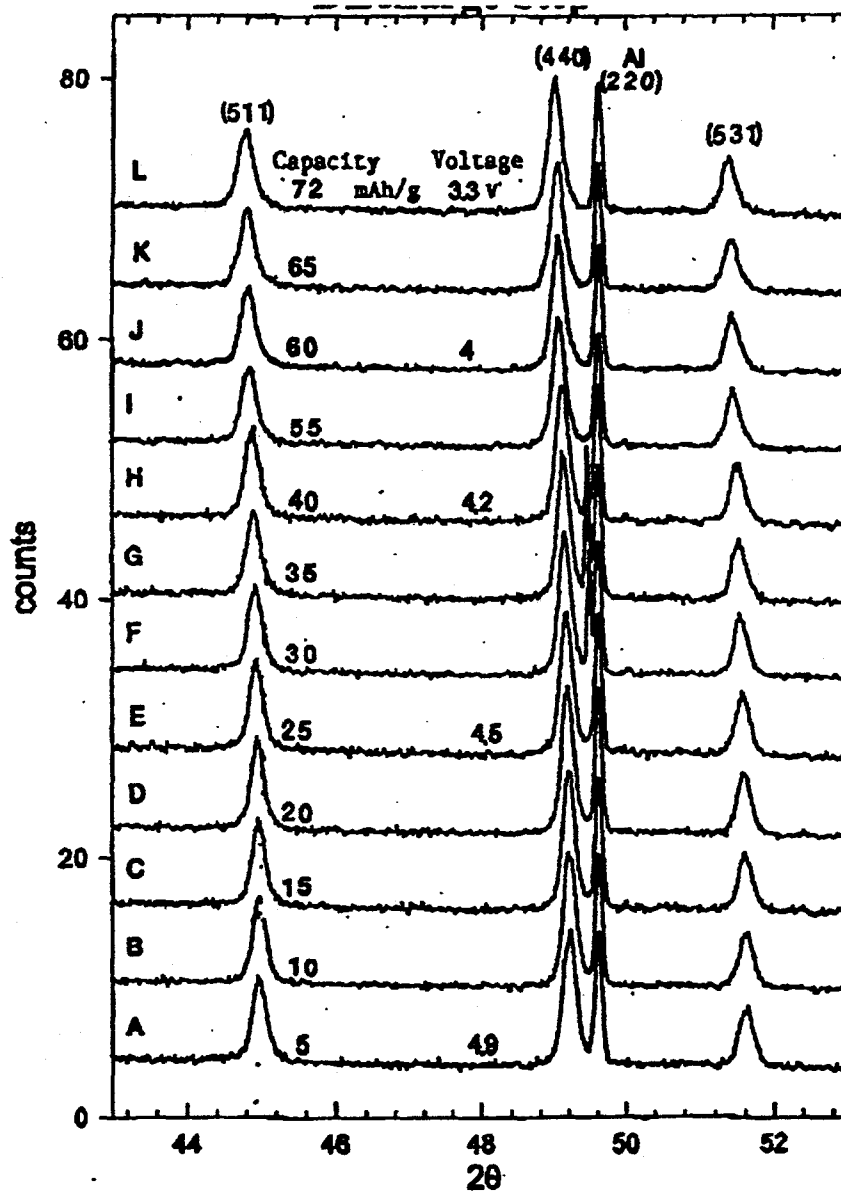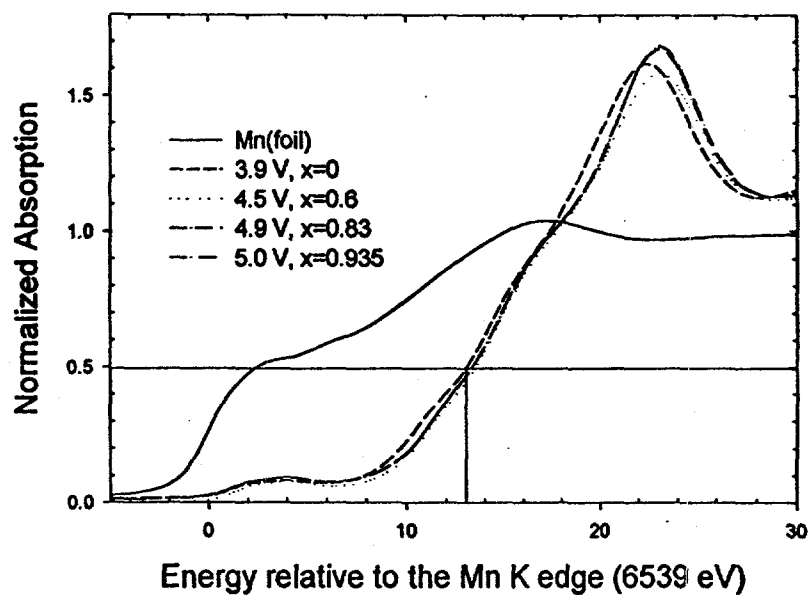Fig. 3. *In situ* XRD patterns on $LiCu_{0.5}Mn_{1.5}O_4$ during the second discharge cycle.

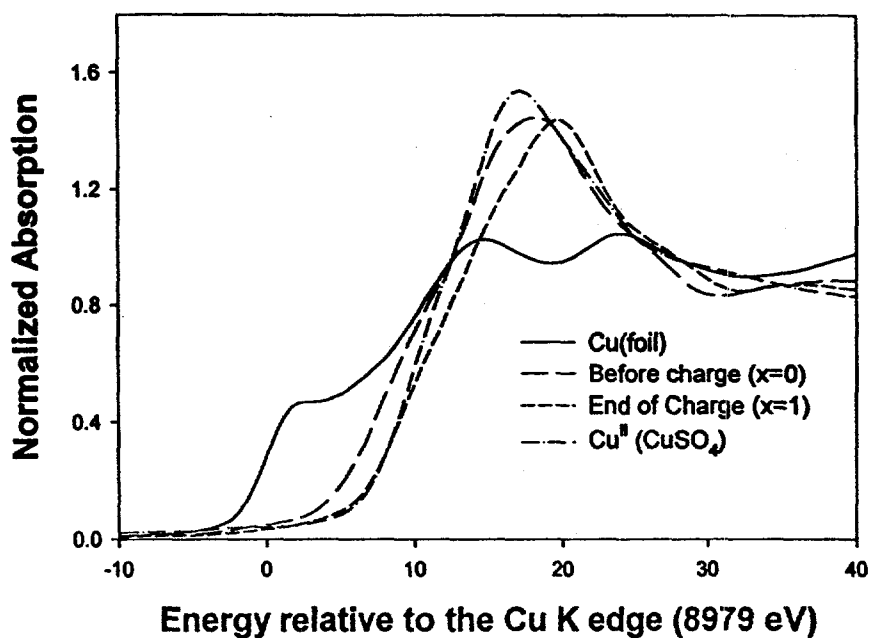Fig. 4. *In situ* XANES at Mn K edge during charge of $Li_xCu_{0.5}Mn_{1.5}O_4$.

Fig. 5. *In situ* XANES at Cu K edge during charge of $Li_xCu_{0.5}Mn_{1.5}O_4$. Data for a Cu foil and a 0.5 M $CuSO_4$ solution are also shown.
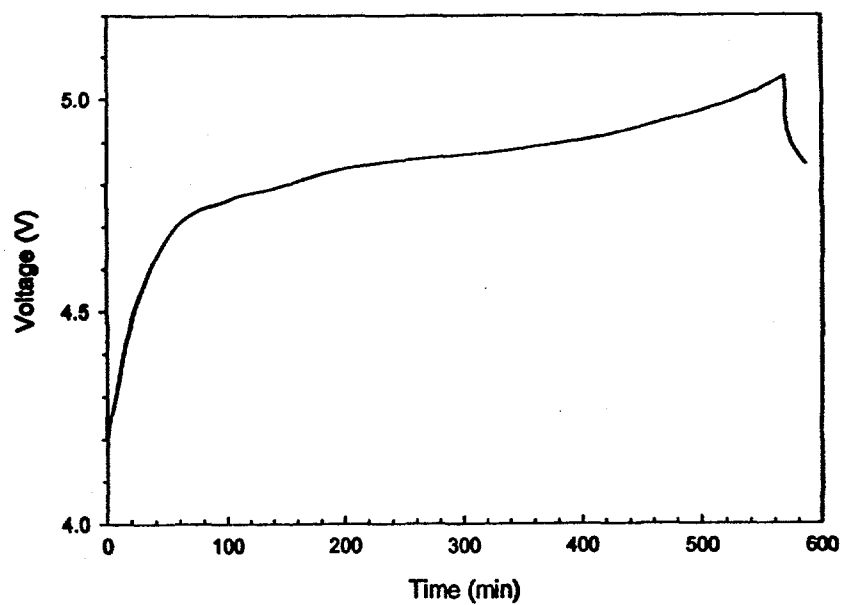
Fig. 6. Charging curve for $LiNi_{0.5}Mn_{1.5}O_4$.
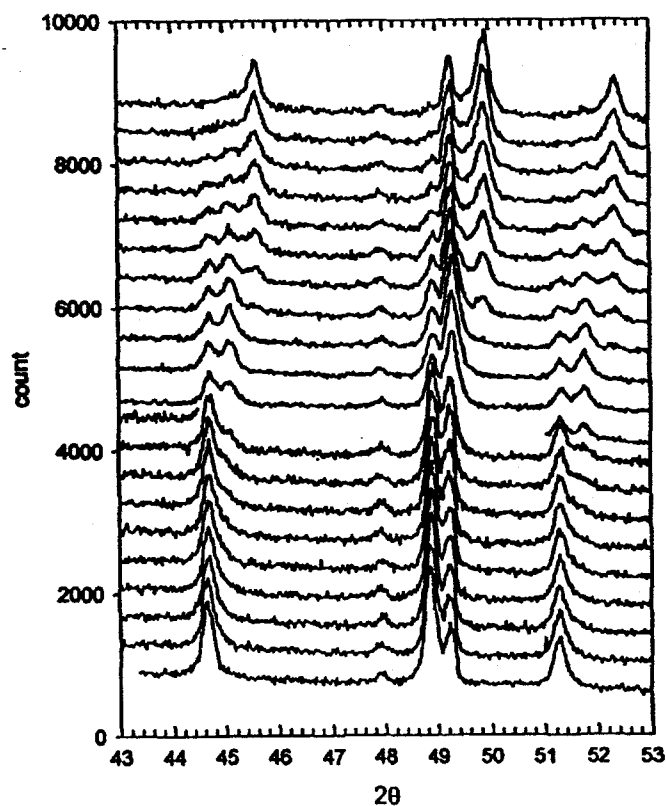
Fig. 7 XRD patterns for second charge of $LiNi_{0.5}Mn_{1.5}O_4$. Beginning of charge at bottom. End of charge at top.
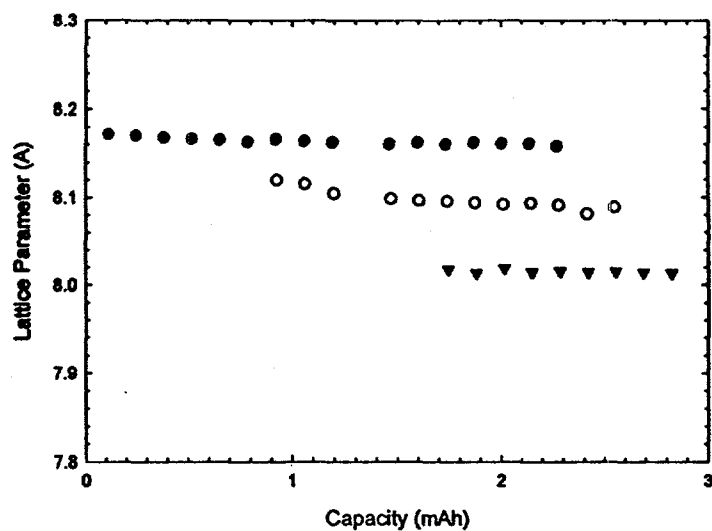
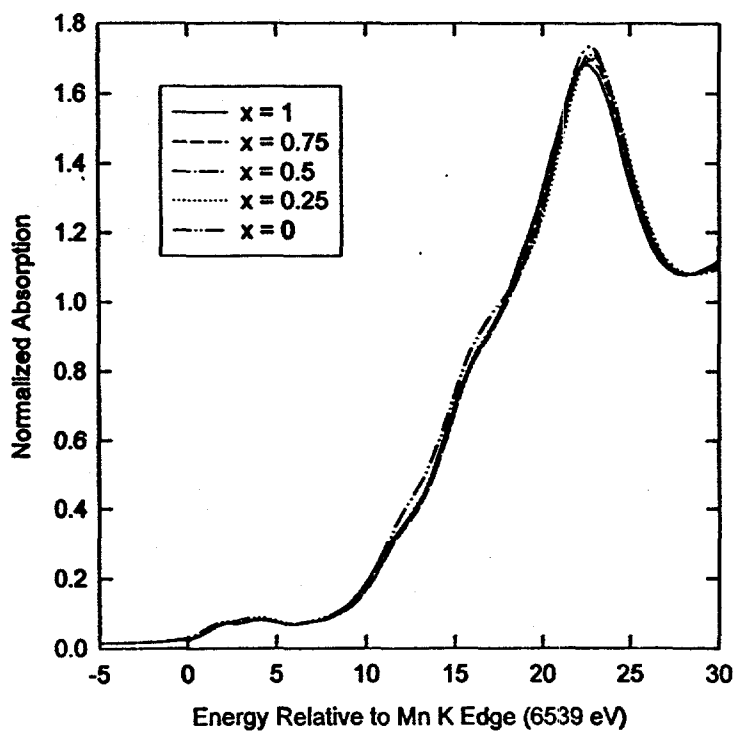Fig. 7. Lattice parameters during charge of $LiNi_{0.5}Mn_{1.5}O_4$.

Fig. 9. Mn K edge XANES during charge of $Li_xNi_{0.5}Mn_{1.5}O_4$.
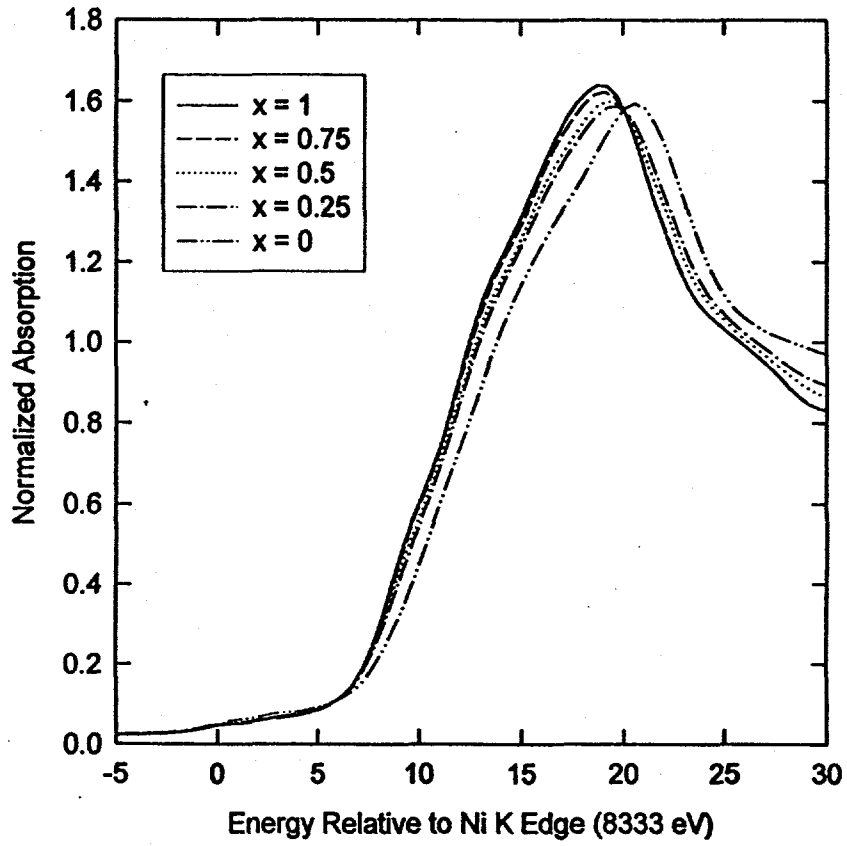
Fig. 10. Ni K edge XANES during charge of $Li_xNi_{0.5}Mn_{1.5}O_4$.